Charge transfer modulation in charge transfer co-crystals driven by crystal structure morphology

Charge transfer modulation in Charge Transfer co-crystal driven by crystal structure morphology

Federica Solano[1], Paolo Inaudi[1]*, Ornella Abollino[1], Agnese Giacomino[1], Mario Chiesa[2], Enrico Salvadori[2], Gabriele Kociok-Kohn[3], Enrico da Como[4]*, Tommaso Salzillo[5], Claudio Fontanesi[6,7]*

[1] *Department of Drug Science and Technology, University of Torino, Via Giuria 9, Torino, Italy*

[2] *Department of Chemistry, University of Torino, Via Giuria 5, Torino, Italy*

[3] *Material and Chemical Characterization Facility (MC2), University of Bath, Claverton Down, Bath BA2 7AY, United Kingdom*

[4] *Department of Physics, University of Bath, BA2 7AY, United Kingdom*

[5] *Department of Industrial Chemistry, University of Bologna, Viale del Risorgimento 4, Bologna, Italy.*

[6] *DIEF, University of Modena and Reggio Emilia, via Vivarelli 10, 41125 Modena, Italy*

[7] *National Interuniversity Consortium of Materials Science and Technology (INSTM), Via G. Giusti 9, 50121 Firenze (FI), Italy.*

Abstract

The electronic properties of a charge-transfer (*donor-acceptor*) semiconducting organic co-crystal, Perylene:F4-TCNQ (PE:F4) (the *donor*, D, is PE, the *acceptor*, A, is 2,3,5,6-Tetrafluoro-7,7,8,8 tetracyanoquinodimethane (F4)) in its 3:2 stoichiometry, are experimentally and theoretically studied. This is done by means of electron paramagnetic resonance (EPR) and solid state electrochemical, cyclic voltammetry (CV), measurements on single crystals. In particular, solid state electrochemistry proves to be an effective tool to probe, on a macroscopic scale, the electronic characteristics of the co-crystal. While, EPR highlights the presence of spin ½ radicals localized on F4 molecules, possibly linked to defects. The experimental findings are discussed on the basis of density functional theory (DFT) based calculations: carried out both using the projector augmented waves (PAW), with "periodic boundary conditions" (pbc), method and the localized orbitals, molecular cluster, approach. In particular, a satisfying agreement is found between the experimental, 0.336 eV (electrochemical), and theoretical, 0.303 eV (PAW), band gap. Differences with the reported optical bandgap are discussed considering excitonic effects.

Keywords: Perylene, F4TCNQ, charge-transfer crystal, EPR, cyclic voltammetry, DFT

e-mail: claudio.fontanesi@unimore.it

Introduction

The interest in the study of charge transfer (CT) co-crystals is due to their peculiar electrical and magnetic properties.[1,2] Initially developed as synthetic metals, *i.e.* conductors based on molecules that can be synthesized in the laboratory, charge transfer co-crystals have recently seen renovated interest as semiconductors with potential ambipolar properties.[3,4] Interest arises from the many applications of semiconductors in devices capable of convert electrical power into light, OLEDs, with a broad spectrum of tunability enabled by the donor or acceptor chemistry, and also electrical devices based on semiconductors such as field effect transistors.[5,6] In addition, the optical properties of such co-crystal semiconductors, combined with their needle like crystal habit, allows for potential applications in photonics as waveguides, where light from an external light source with energy below the gap, or the luminescence of the co-crystal can be guided.[7] Crucial to the many possible applications of these materials as semiconductors are the energy values of the frontier orbitals, i.e. the energies of the highest occupied molecular orbital (HOMO) and lowest unoccupied molecular orbital (LUMO).[8–11] In a parallelism with conventional inorganic semiconductors, these correspond to the valence and conduction band, respectively. As for single component organic semiconductors, *e.g.* pentacene, rubrene, oligo-thiophenes, etc., the energy of the HOMO and LUMO levels are crucial since, not only they determine the electronic gap of the material itself, but also represent the energetics barriers with respect to the electrode work-functions in metal-semiconductor junctions and thus they are parameters that strongly influence the contact resistance and performance in the devices. Photoemission spectroscopy and inverse photoemission have been extensively used to determine HOMO and LUMO levels of organic semiconductors in the form of thin films.[12]. However, single crystals, being the most ordered system with minimal concentration of grain boundaries, remain a benchmark in terms of studying the intrinsic properties of a new molecular material and often display the best performance in terms of charge carrier transport..[5,13] There are only few photoemission studies on organic single crystals and even fewer on charge transfer co-crystals one of the reasons being the likelihood of surface charging effect in the photoemission experiment, giving spurious effects.[14,15] Charge transfer co-crystals arise from the combination of two closed shell neutral molecules in which the HOMO and LUMO levels that are offset to promote a transfer of charge from a donor, D, to the acceptor, A. This occurs from having the energy of both these frontier orbitals close to the vacuum level for D compared A. The transfer of charge from D to is the process responsible for the formation of a D-A pair.[16,17] Then semiconducting properties of D:A co-crystals are mainly connected to the presence of a delocalized π-conjugated systems, and by the presence of hetero-atoms and/or substituent groups able to suitably modulate the energy offset of molecular orbitals of D and A, hence the overall electronic structure and degree of charge transfer, ρ.[18,19]

We and other research groups have demonstrated how ρ is also a function of the molecular geometrical arrangement in the crystalline structure and by the stoichiometry of the co-crystal.[18,19] In principle, D_n:A_m could assume any stoichiometric value.[20,21] Charge transfer complexes with semiconducting properties show the most common 1:1 stoichiometry and a stacking geometry in which D and A alternate in sandwich fashion along the stacking direction (A-D-A-D). This is known as an alternated stack co-crystal.[22,23] The high electron affinity

(EA) of the acceptor and the low ionization energy (IE) of the donor generate a dimer, or pair, characterized by a band-gap, defined as a first approximation by the difference between the energy of the acceptor's LUMO and the donor's HOMO.[24–26] But in an energetically more complex system characterized by long range periodicity, such as a co-crystal, the electronic coupling between the HOMO of D and the LUMO of A plays a major role in determining ρ, which may result in partial ionicity of the system $D^{\rho+}$-$A^{\rho-}$, i.e. $0 < \rho < 1$. This is a parameter that is widely used to classify these molecular material class. Charge transfer co-crystals with low charge transfer degree $\rho < 0.5$, thus partially ionized molecules, typically show semiconducting properties.[27,18,17] Single component organic semiconductors show band gap energies (E_{BG}) between 0.8 and 3 eV which is limiting when considering applications in infrared optoelectronics or thermal imaging. Semiconducting co-crystal can overcome such limitations since the bandgap can be tuned by a judicious choice of the D and A molecules, but ways to characterize their electronic bandgap in the solid state and the degree of charge transfer are still a very important topic at the centre of the development of such materials. In this work we characterize the electronic structure of the charge transfer co-crystal obtained from pairing 2,3,5,6-Tetrafluoro-7,7,8,8 tetracyanoquinodimethane (F4) as A and perylene (PE) as D.[18,28,29] PE:F4 crystallizes in the uncommon, and structurally non trivial 3:2 stoichiometry. The main aim is to provide information on the electronic bandgap via solid state electrochemical measurements, such as cyclic voltammetry (CV) performed in solution and on the single crystals. We report a quasi-reversible behaviour in CV, which is consistent with valuable conductive properties. The solid state electrochemistry approach allows to extract information directly on the solid and thus relevant for solid state devices.[30–32] The energy of HOMO, LUMO and the related band-gap are compared with the experimental optical band gap reported by us in literature[18] and to theoretical calculations. showing a fairly good agreement. EPR experiments show the presence of a doublet state, which can be assigned to F4 radical anions. Results are compared to a similar study on dibenzotetrathiafulvalene/2,3,5,6-tetrafluoro-7,7,8,8-tetracyanoquinodimethane (DBTTF:F4) co-crystals, where the degree of charge transfer correspond to one, i.e. a fully ionic system.[33–35]

Experimental

Chemicals

Perylene 99% purity (PE) was purchased from Sigma-Aldrich, and 2,3,5,6-tetrafluoro-7,7,8,8-tetracyanoquinodimethane 98% purity (F4) was purchased from TCI-UK. The materials were purified by vacuum sublimation. Acetonitrile anhydrous, ACN (<99 % purity), tetrabutylammonium hexafluorophosphate, TBAPF6 (99% purity) and Nafion 117 solution 5% were obtained from Sigma-Aldrich and were used for electrochemical studies. During all electrochemistry analyses alumina powder was used to renew electrode surface. All the glassware was boiled in nitric acid and then cleaned by rinsing in high purity water, Millipore (resistivity > 20 MΩ cm).

Charge Transfer (CT) co-crystal growth.

PE:F4 co-crystals were grown using a horizontal tube furnace under argon stream. Argon gas was obtained from BOC-UK with a purity of 6 N. A 2 m long quartz tube was filled with smaller diameter tubes of 10 cm length each. Those were used to harvest the crystals at the end of the growth procedure. The small tubes were cleaned by ultrasonication in successive steps with deionized water, 2-propanol and acetone. About 150 mg of each material were placed in a Carbolite EHC 12/600B three zone furnace with the hot zone at 537 K, the centre of the furnace at 460 K and the cold zone at 410 K. Further details on the crystal growth system can be found in previous works.[23,36]

EPR

Room temperature X-band (9.8 GHz) CW-EPR spectra were collected on a Bruker EMX equipped with a super-high Q resonator (ER4122 SHQE). Low temperature Q-band (33.8 GHz) CW-EPR spectra were collected on a Bruker ELEXSYS E580 using an EN 5107D2 Bruker resonator housed in an Oxford CF935 cryostat. All samples were finely grinded in order to obtain a powder averaged spectrum. Spectra simulations were performed using EasySpin 5.2.28 toolbox[37] within the Matlab 2019b software suite (The Mathworks Inc., Natick, MA).

Electrochemical set-up

The electrochemical measurements were performed using a PalmSens3 portable potentiostat (PalmSens, Houten, Netherlands), driven by using the PSTrace 4.6 software. The latter was used both to set the process parameters and record the experimental data. A conventional three electrode cell was used for electrochemical studies of pristine solutions. The working electrode (WE) was a glassy carbon electrode (GCE) with a diameter of 3 mm. The counter electrode (CE) was a Pt electrode. The potentials were measured against an $Ag/AgCl/KCl_{sat}$ reference electrode (RE). A peculiar arrangement was adopted in the case of co-crystals to preserve their solid state: a cylindrical Teflon cell featuring a hole (0.8 cm diameter) in the bottom was used in a vertical configuration. A glassy carbon electrode (size: 25 mm x 25 mm x 0.5 mm) was tightened from below to a copper plate as the electrical contact (WE); a Teflon ring was used to ensure no solution leakage from the cell. While a Pt wire and an $Ag/AgCl/KCl_{sat}$ were used as CE and RE, respectively. The co-crystals were placed on the WE and covered with a Nafion membrane. The latter was maintained in air contact for 5 minutes, eventually the electrolytic solution was added. The Nafion membrane is exploited to prevent direct contact between the solid co-crystal and the electrolytic solution avoiding the dissolution of the co-crystals, but preserving the ion transfer. In fact, if dissolved in solution, the co-crystals would dissolve yielding the pristine neutral PE and F4species. Further details on the solid state electrochemical setup can be found in ref. [51].

Calculation details

Theoretical results presented and discussed in the main manuscript are obtained by using the VASP 5.4.4 program. Calculations are run within the General Gradient Approximation (GGA) of the density functional theory with periodic boundary conditions (pbc).[38,39] We use projector augmented waves (PAW)[40] pseudopotentials with exchange correlation functionals as parameterized by Perdew-Burke-Ernzerhof (PBE), with a cut-off energy of 400 eV. Atomic coordinates were relaxed using the conjugate-gradient method starting from the structural parameters obtained by x-ray,[18] with Monkhorst-Pack k-point samplings of 5 × 3 × 3. For comparison, localized orbitals calculations are carried out within the framework of ab-initio linear combination of atomic orbitals (LCAO) using FireFly, GAMESS and ORCA suite of programs.[41–43] This localized orbitals approach has been performed using the B3LYP and CAM-B3LYP functionals, and post-HF MP2 method, 6-31G(d) as basis-set. Localized orbitals calculations concerning the crystal were performed by extraction of a "cluster" of molecules (a trimer formed by two perylene and one F4TCNQ molecules) maintaining fixed the experimental geometrical disposition exactly as obtained by X-rays diffraction data analysis. Results obtained by using localized orbitals calculations are reported, and concisely assessed, in the Supporting Information. Plane waves post-scf data elaboration and graphs are obtained by using the XCrySDen,[44,45] VESTA,[46] mcu0.2[47] and Bader packages.[48–50]

Results and Discussion

Electrochemical behaviour of pristine F4 and PE

Figure 1 sets out CVs of PE in bulk solution. A first weak and shallow current peak showing a quasi-reversible behaviour is present at about +0.5 V in the forward oxidation curve. As the potential is scanned more positive, a much more complicated pattern is observed in the +1.0 to +1.8 V potential range. Moreover, the current potential curves result a function of the scan rate: two oxidation peaks, of irreversible nature, are evident at slow scan rates, they merge in a single current peak centred at about 1.2 V with a 100 mV s^{-1} potential scan rate. The latter oxidation peak is likely due to follow-up chemical reactions, possibly leading to the formation of a PE-based polymer, and indeed the WE surface appears covered by a thin film, whose study relating to the film-formation and characterization is in progress in this lab. Figure 1 inset shows CV curves recorded in a narrower potential window, the potential is scanned between 0.1 and 0.8 V, showing a quasi-reversible electrochemical behaviour, which is thus limited to the first oxidation step. Indeed, in the case of PE few electrochemical studies are present in the literature and this paper reports for the first time perylene CV curves.[51] Table I summarizes the electrochemical results of the pristine PE and F4 compounds, at 50 mV s^{-1} potential scan rate (negligible variations are found at 20 and 100 mV s^{-1}, please compare the Supporting Information section). CVs of pristine F4 were reported previously.[52]

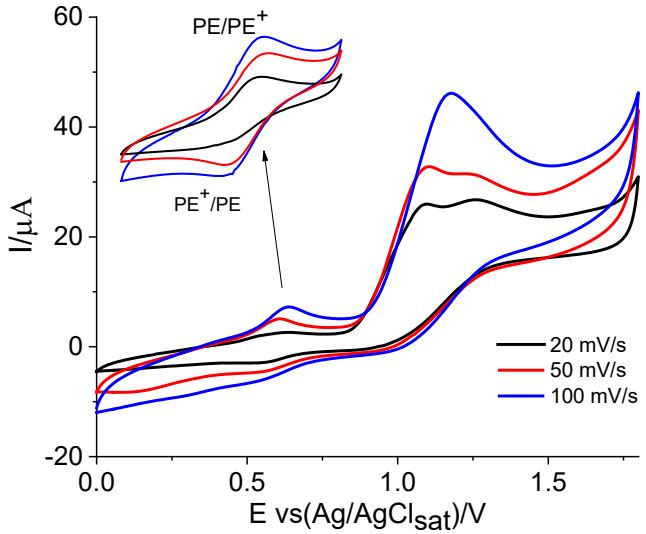

Figure 1. Cyclic voltammetry of pristine PE in 0.1 $TBAPF_6$ ACN solution containing: 1 mM PE. WE: GCE, RE: $Ag/AgCl/KCl_{sat}$, CE: Pt wire. Black, red and blue curves were obtained at 20, 50, 100 mV s^{-1} scan rate, respectively.

Table I. Anodic peak potential (E_{pa}), cathodic peak potential (E_{pc}), the relevant difference (ΔE), and *HOMO/LUMO* energy values. Electrochemical values obtained by elaborating CVs obtained at a 20 mV s^{-1} potential scan rate.

20 (mV s^{-1}) *scan rate*	E_{pa} *(V)*	E_{pc} *(V)*	ΔE *(V)*	*HOMO (eV)*	*LUMO (eV)*
$F4_{(sol)} + e^- \rightleftharpoons F4^-_{(sol)}$	0.640	0,543	0.097		-5.167
$F4^-_{(sol)} + e^- \rightleftharpoons F4^{2-}_{(sol)}$	0.153	0.062	0.091		
$PE_{(sol)} \rightleftharpoons PE^+_{(sol)} + e^-$	0.613	0.546	0.067	-5.052	

Solid-state electrochemistry

Figure 2 shows CV voltammograms recorded in the case of the PE:F4 co-crystal. A carbon-paste electrode (CPE) is used as WE, a Pt wire the CE, Ag/AgCl KCl is the RE.

Examination of CV curves reported in Figure 2 allow for a close comparison between the electrochemical behaviour of the pristine F4 and PE compounds in solution (Figure 2a) and the CV pattern obtained in the solid-state electrochemistry setup (Figure 2b). CVs of PE in the solid state are also shown in Figure 2c.

In the +0.7 to +1.8 V range (black line, Figure 2b), the PE:F4 CV parallels the pristine PE results (red line, Figure 2c). Two broad oxidation current peaks are present in the oxidative scan at around +1 and +1.3 V. The latter CV peaks show a totally irreversible nature. In the -0.5 to 0.8 V potential range (black line, Figure 2b) very shallow broad shoulders are present, the relevant current values are almost negligible with respect to the current of the oxidation peaks.

CVs recorded starting at the open circuit potential (OCP) are also shown in Figure 2b: red and blue curves are the anodic and cathodic scans, respectively. Previous studies showed that the PE:F4 co-crystal features a limited charge transfer character ($\rho < 0.5$) ref [18]. Where PE is found positively charged and complementarily F4

has negative charge density with ρ of about 0.3. This is different with respect to the fully ionic co-crystal DBTTF:F4.[52] Due to the known limited charge transfer in the PE:F4, the peak in the anodic scan at about +0.65 V (red line, in Figure 2b) can be tentatively assigned to the PE oxidation (which corresponds to swallow current features found in the -0.5 to 1.6 V CV – black line in Figure 2b). The reduction of the F4 to the $F4^{-}$ anion species is the redox process underlying the reduction peak at about -0.05 V (blue line in Figure 2b). While the couple of broad peaks found at about +1.0 and +1.25 V in the wide range potential scan (black line in Figure 2b) can be assigned to the PE oxidation. The latter peaks are extremely similar to the couple present in the pristine PE CVs, compare with Figure 2(b) black curve (20 mV/s potential scan rate). In addition, we stress that the peak-to-peak current difference in the blue CV, Figure 2b, is about four time the peak-to-peak current difference in the red CV. This suggests a more efficient redox process concerning the reduction of the F4 species compared to the PE oxidation. Such an experimental evidence can be due to a much more efficient intermolecular charge transmission along the PE network of molecules (which forms a continuous sub-lattice within the PE:F4 crystal), with respect to the possible oxidation of the $F4^{-}$ anion (F4 sites within the PE:F4 crystal are isolated as further discussed in Figure 4). Moreover, F4 is present as a species bearing a slightly negative charge $F4^{\delta-}$ rather in its anionic form.

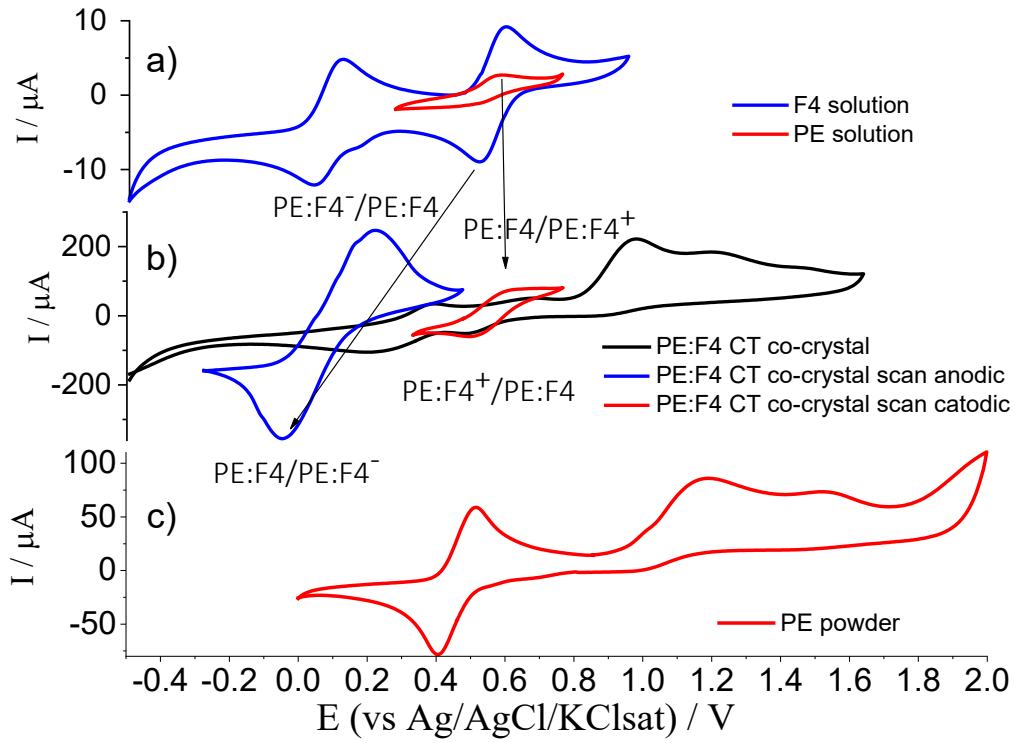

Figure 2. a) CVs of the pristine F4 and PE compounds in $TBAPF_6$ ACN solution with GCE as the WE. b) CVs recorded of the PE:F4 co-crystal, same condition as in Figure 1. c) CV of the pristine powder PE covered with a Nafion membrane, $TBAPF_6$ ACN solution, GCE is the WE, a Pt wire is the CE, Ag/AgCl/KCl is the RE. 20 mV s^{-1} is the potential scan rate.

Table II summarizes the solid-state electrochemistry E_{pa}, E_{pc}, ΔE, *HOMO- LUMO* and *band gap* values obtained by elaboration of the PE:F4 CVs shown in Figure 1 and Figure 2, respectively. This together with the estimated *HOMO, LUMO* and *band gap* values.

Table II. Potential of anodic peak (E_{pa}), potential of cathodic peak (E_{pc}), the correspondent difference (ΔE), and *HOMO/LUMO* energy values obtained using a scan rate of 20 mV s^{-1}.						
20 (mV s^{-1}) *scan rate*	E_{pa} *(V)*	E_{pc} *(V)*	ΔE *(V)*	*HOMO (eV)*	*LUMO (eV)*	*band gap (eV)*
$PE{:}F4_{(solid)} \rightleftharpoons PE{:}DB^{+}_{(solid)} + e^{-}$	0.640	0.533	0.107	-4.832		0.336
$PE{:}F4_{(solid)} + e^{-} \rightleftharpoons PE{:}F4^{-}_{(solid)}$	0.238	-0.046	0.284		-4.496	

We compare the results of the performed CV measurements with the optical band gap reported for the 3:2 stoichiomorph of PE:F4 reported in our previous work.[18] As shown previously the structure is characterized by a dimer stack D-A along the crystal growth direction corresponding to the *a* axis and a trimer stack DAD almost parallel to the *c* axis. Thus the 3:2 stoichiomorph shows two, perpendicularly polarized to each other, optical absorption having onset of the charge transfer excitons at 0.68 eV for the dimer and 0.77 eV for the trimer. The band gap from CV measurements is 0.336 eV, thus lower with respect to what has been estimated by optical spectroscopy. Such difference is not surprising considering that in optical experiments the energy difference across the gap is obtained through the observation of a neutral excitation, excitons, while in CV charges are injected at the interface of the crystal with possible polarization effects.

EPR characterization

The EPR powder spectrum of the PE:F4 co-crystals was recorded in the X-and Q-band frequencies ranges, both at room temperature and at 50 K (Figure 3) and proved to be independent of temperature in this range. At both frequencies the spectrum is characterized by a nearly isotropic resonance line centred at $g = 2.00$. Computer simulation of the spectrum at the two frequencies (red lines in Figure 3) indicates a small anisotropy of the **g** tensor (**g**=[2.0033 2.0033 2.0037]±0.0001) in line with computed values for the F4 radical anion, which represents the defective trapping sites in this system. No evidence is found for spin states higher than *S*=1/2 up to room temperature (Figure 3a). Taken together these evidences point to the existence of ground-state F4 radical anions within the PE:F4 co-crystal. Possibly the existence of F4 radical anions is connected to defective sites within the crystal.

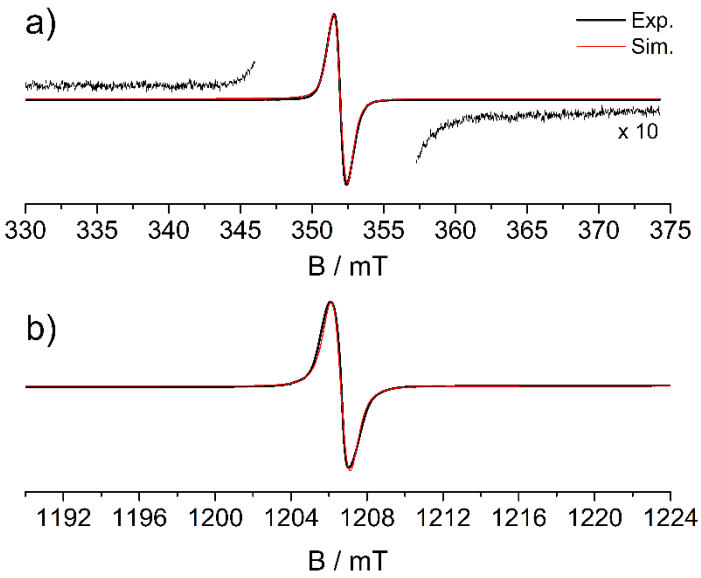

Figure 3 Experimental (black) and simulated (red) CW-EPR spectra of PE:F4 recorded at a) X-band frequency (9.8 GHz) and room temperature. The magnified portions of the spectrum in panel a) demonstrate that no spin states higher than ½ are detectable. Experimental parameters: microwave power = 1mW; modulation amplitude = 0.1 mT. b) Q-band frequency (33.8 GHz) and 50 K. Experimental parameters: microwave power = 0.01 mW; modulation amplitude = 0.1 mT.

Theoretical results

Theoretical calculations are exploited to gain physical insight on the interactions active between the donor-acceptor molecular partners, within the co-crystal. We will pay particular attention to the band gap and the intermolecular (donor-acceptor) charge distribution. The electrochemical behaviour provides a direct information on the band gap, while charge separation properties will be compared to our previous estimates based on IR spectroscopy and the EPR measurements reported above. Modelling of the PE:F4 co-crystal electronic properties is carried out by using both the projector augmented wave (PAW) method and localized orbitals (molecular cluster model reported in the Supporting Information section). PAW calculations for geometry optimization are carried out considering a $5x3x3$ Monkhorst-Pack k-point sampling and in the following conditions: *i*) the geometry parameters fixed to those obtained by single crystal x-ray diffraction *ii*) relaxing the PE and F4 atomic positions, with unrelaxed, *i.e.* experimental, unit cell lattice parameters *iii*) full relaxation of the system allowing for both optimization of atomic position, as well as unit cell lattice parameters. Upon full geometry relaxation, the unit cell volume varies from 2854 $Å^3$ to 2731 $Å^3$ which appears a reasonably small-scale variation. For "final" electronic structure calculation $6x6x6$ Monkhorst-Pack **k**-point sampling was chosen yielding a band gap value of 0.414, 0.346 and 0.303 eV for cases *i*), *ii*) and *iii*), respectively. This outcome compares rather well with the 0.336 eV electrochemical result (*vide supra*, Table II). Figure 4 shows in panel (a) the band structure for the fully relaxed geometry, while in panel (b) a 2D charge density projection on the PE and F4 molecular planes is shown. A clear localization of negative charge surrounding the nitrogen and fluorine ions can be noticed on the F4 molecules. Further viewpoints are shown in panels (c) and (d). The

elaboration of the charge density distribution, following the charge density decomposition method of Bader[48,49,53], allows to calculate the net charge localized on the F4 molecule. The latter results indicate a charge density of −0.69 electrons, after molecular geometries and cell lattice constants relaxation (*i.e.* full relaxation); −0.58 and −0.63 values are obtained for the experimental un-relaxed and molecular-only relaxed geometries, respectively. The calculated net charge localized on F4 molecule is just larger than the experimental one, -0.3, estimated by IR spectroscopy ref.[18]. Figure 4 summarizes "at-a-glance" the essential electronic properties of the PE:F4 co-crystal, calculated by using the PAW based density functional method. Figure 4a shows the band-structure as a function of the k-path distance, the minimum band-gap energy is at Γ, Figure 4b sets out the relevant high-symmetry points. Figure 4 c and d show two-dimensional projections of the electron localization function (ELF). In particular, Figure 4c shows ELF 2D projections on two planes coplanar with facing F4 and PE molecules, whilst Figure 4d shows ELF 2D projections on a plane roughly orthogonal to the previous ones. The latter is passing through sp_2 carbons of a PE-F4-PE cluster, red area are evident between carbon carbon double bonds (intramolecular covalent bonds), remarkably the intermolecular area is deep blue indicating the absence of any significant intramolecular chemical interaction (i.e. there is no evidence of any π π stacking chemical interaction).

<table>
<tr><td>a)</td><td>b)</td></tr>
<tr><td> 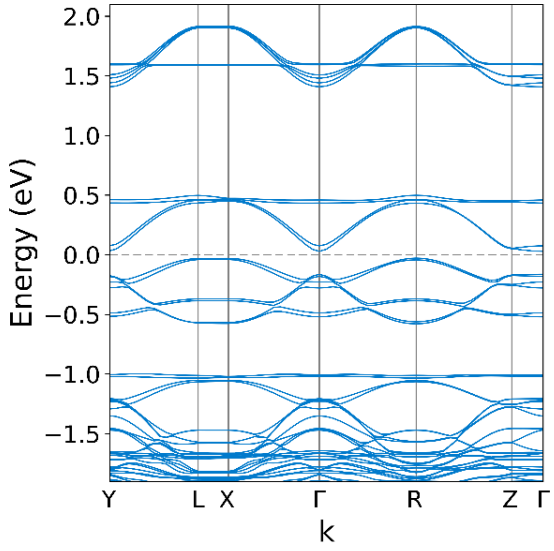
</td><td> 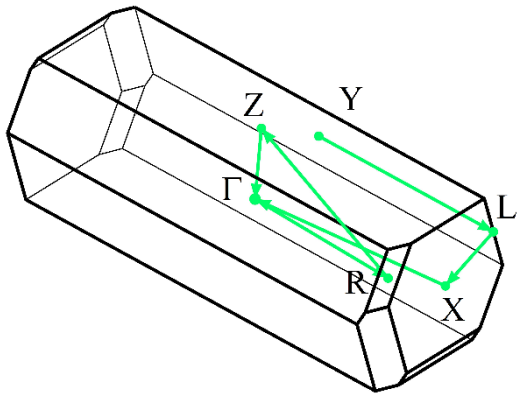
</td></tr>
<tr><td>c)</td><td>d)</td></tr>
</table>

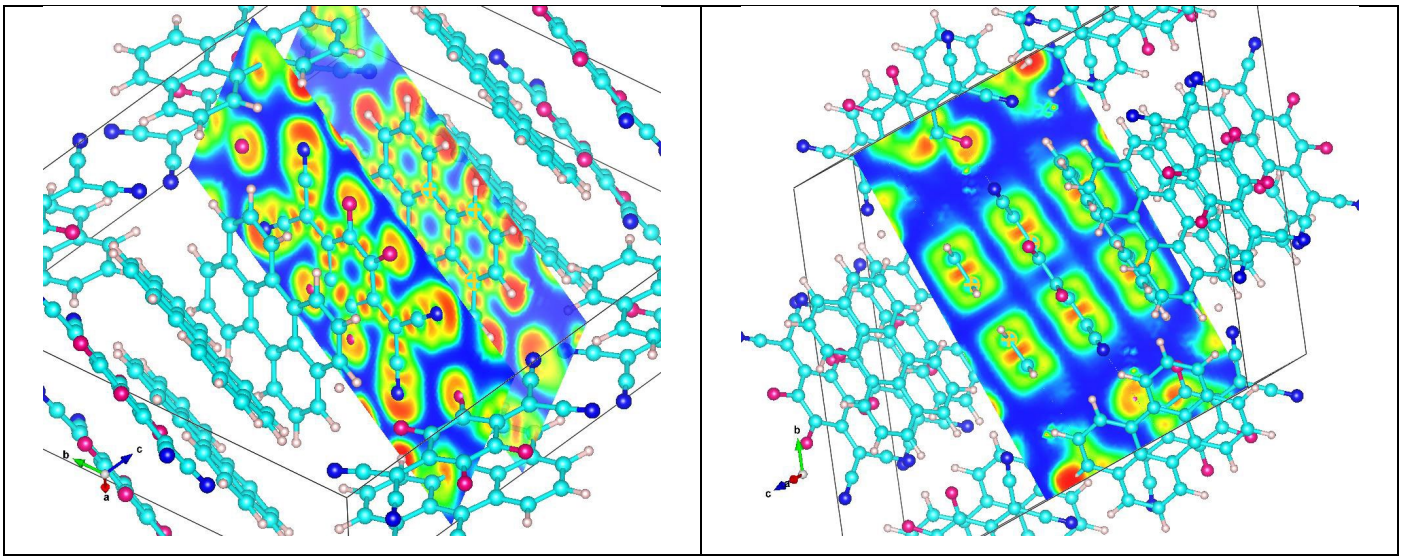

Figure 4. a) Band structure plot vs. K-point distance, Y–L–X–Γ–R–K–Z–Γ K–path b) Details of the selected high symmetry K-points.[44] c) $6x6x6$ Monkhorst–Pack PBE full-relaxed geometry: 2D projected ELF plot, red colour bonding (or lone couple) region, deep blue ELF = 0, i.e. low electron density.

Conclusions

Integration and comparison of the information obtained by x-ray, EPR and CV experimental results, with theoretical DFT based calculations allowed us for obtaining some thoroughly insights on PE:F4 electronic structure and the degree of charge-transfer in the solid-state. The comparison of the experimental overall picture and theoretical outcome suggests that PE:F4 features a degree of charge transfer certainly lower than one. From calculations a singlet ground state is the most stable, where the F4 appears negatively charged, with values in the range – 0.58 to -0.7 and the material shows an electronic bandgap in good agreement with what is measured as the HOMO LUMO separation by electrochemistry. However, EPR experiments point towards a localized spin ½ radical. In light of the crystal structure with F4 molecules essentially isolated when compared to the network of PE molecules, mainly because of the trimers, it is not unreasonable that some F4 molecules in structural defects may take a charge of -1 and dominate the EPR signal. We speculate that the PE network substructure may be characterized by a very efficient charge transport mechanism, as the analysis of the electrochemical data suggest.

Peculiar differences emerge between PE:F4 co-crystals and the DBTTF:F4 cocrystals studied by our group with similar techniques.[52] Such differences can be related to the electronic characteristics of the molecular arrangement in the solid-state. The comparison between DBTTF:F4 and PE:F4 co-crystals electronic properties as inferred from the analysis of experimental and theoretical data strongly indicates a decisive role played by the crystal structure, segregated stack in DBTTF:F4 compared to the alternating almost herringbone arranged stacks in PE:F4.

Acknowledgements

C.F. gratefully thanks financial support from Dipartimento di Ingegneria “Enzo Ferrari” (DIEF), UniMORE, FARD 2021 - linea di azione di tipo 3: “Materiali chirali per batterie al litio e celle a combustibile” and from Consorzio Interuniversitario Nazionale per la Scienza e Tecnologia dei Materiali (INSTM), fondi triennali: “INSTM21MOFONTANESI”.

References

1 M. Pope, H. P. Kallmann and P. Magnante, Electroluminescence in Organic Crystals, *J. Chem. Phys.*, 1963, **38**, 2042–2043.

2 M. Pope and C. E. Swenberg, *Electronic Processes in Organic Crystals and Polymers*, Oxford University Press 1982, Oxford, 1982.

3 H. Huang, Z. M. Strater, M. Rauch, J. Shee, T. J. Sisto, C. Nuckolls and T. H. Lambert, Electrophotocatalysis with a Trisaminocyclopropenium Radical Dication, *Angewandte Chemie International Edition*, 2019, **58**, 13318–13322.

4 T. Salzillo, A. Campos and M. Mas-Torrent, Solution-processed thin films of a charge transfer complex for ambipolar field-effect transistors, *J. Mater. Chem. C*, 2019, **7**, 10257–10263.

5 V. Podzorov, M. E. Gershenson, Ch. Kloc, R. Zeis and E. Bucher, High-mobility field-effect transistors based on transition metal dichalcogenides, *Appl. Phys. Lett.*, 2004, **84**, 3301–3303.

6 L. Fijahi, T. Salzillo, A. Tamayo, M. Bardini, C. Ruzié, C. Quarti, D. Beljonne, S. d’Agostino, Y. H. Geerts and M. Mas-Torrent, Charge transfer complexes of a benzothienobenzothiophene derivative and their implementation as active layer in solution-processed thin film organic field-effect transistors, *Journal of Materials Chemistry C*, 2022, **10**, 7319–7328.

7 J. Wang, S. Zhang, S. Xu, A. Li, B. Li, L. Ye, Y. Geng, Y. Tian and W. Xu, Morphology-Dependent Luminescence and Optical Waveguide Property in Large-Size Organic Charge Transfer Cocrystals with Anisotropic Spatial Distribution of Transition Dipole Moment, *Advanced Optical Materials*, 2020, **8**, 1901280.

8 J. L. Bredas and S. Marder, *The WSPC Reference on Organic Electronics: Organic Semiconductors*, World Scientific Publication Co., Singapore, 2016.

9 D. Vanossi, L. Cigarini, A. Giaccherini, E. da Como and C. Fontanesi, An Integrated Experimental/Theoretical Study of Structurally Related Poly-Thiophenes Used in Photovoltaic Systems, *Molecules*, 2016, **21**, 110.

10 R. Noriega, J. Rivnay, K. Vandewal, F. P. V. Koch, N. Stingelin, P. Smith, M. F. Toney and A. Salleo, A general relationship between disorder, aggregation and charge transport in conjugated polymers, *Nat Mater*, 2013, **12**, 1038–1044.

11 I. Salzmann, G. Heimel, M. Oehzelt, S. Winkler and N. Koch, Molecular Electrical Doping of Organic Semiconductors: Fundamental Mechanisms and Emerging Dopant Design Rules, *Acc. Chem. Res.*, 2016, **49**, 370–378.

12 S. R. Forrest and M. E. Thompson, Introduction: Organic Electronics and Optoelectronics, *Chem. Rev.*, 2007, **107**, 923–925.

13 T. Salzillo, A. Campos, A. Babuji, R. Santiago, S. T. Bromley, C. Ocal, E. Barrena, R. Jouclas, C. Ruzie, G. Schweicher, Y. H. Geerts and M. Mas-Torrent, Enhancing Long-Term Device Stability Using Thin Film Blends of Small Molecule Semiconductors and Insulating Polymers to Trap Surface-Induced Polymorphs, *Advanced Functional Materials*, 2020, **30**, 2006115.

14 H. Kakuta, T. Hirahara, I. Matsuda, T. Nagao, S. Hasegawa, N. Ueno and K. Sakamoto, Electronic Structures of the Highest Occupied Molecular Orbital Bands of a Pentacene Ultrathin Film, *Phys. Rev. Lett.*, 2007, **98**, 247601.

15 S. Machida, Y. Nakayama, S. Duhm, Q. Xin, A. Funakoshi, N. Ogawa, S. Kera, N. Ueno and H. Ishii, Highest-Occupied-Molecular-Orbital Band Dispersion of Rubrene Single Crystals as Observed by Angle-Resolved Ultraviolet Photoelectron Spectroscopy, *Phys. Rev. Lett.*, 2010, **104**, 156401.

16 A. Das and S. Ghosh, Supramolecular Assemblies by Charge-Transfer Interactions between Donor and Acceptor Chromophores, *Angewandte Chemie International Edition*, 2014, **53**, 2038–2054.

17 L. Sun, W. Zhu, F. Yang, B. Li, X. Ren, X. Zhang and W. Hu, Molecular cocrystals: design, charge-transfer and optoelectronic functionality, *Phys. Chem. Chem. Phys.*, 2018, **20**, 6009–6023.
18 T. Salzillo, M. Masino, G. Kociok-Köhn, D. Di Nuzzo, E. Venuti, R. G. Della Valle, D. Vanossi, C. Fontanesi, A. Girlando, A. Brillante and E. Da Como, Structure, Stoichiometry, and Charge Transfer in Cocrystals of Perylene with TCNQ-Fx, *Crystal Growth & Design*, 2016, **16**, 3028–3036.
19 P. Hu, K. Du, F. Wei, H. Jiang and C. Kloc, Crystal Growth, HOMO–LUMO Engineering, and Charge Transfer Degree in Perylene-FxTCNQ (x = 1, 2, 4) Organic Charge Transfer Binary Compounds, *Crystal Growth & Design*, 2016, **16**, 3019–3027.
20 O. Kataeva, K. Ivshin, K. Metlushka, K. Nikitina, V. Khrizanforova, Y. Budnikova, R. R. Fayzullin, S. Latypov, S. Schiemenz, M. Bretschneider, A. Popov, S. Avdoshenko, Y. Krupskaya, B. Büchner and M. Knupfer, New Charge Transfer Cocrystals of F2TCNQ with Polycyclic Aromatic Hydrocarbons: Acceptor–Acceptor Interactions and Their Contribution to Supramolecular Arrangement and Charge Transfer, *Crystal Growth & Design*, 2022, **22**, 751–762.
21 D. Wang, X. Kan, C. Wu, Y. Gong, G. Guo, T. Liang, L. Wang, Z. Li and Y. Zhao, Charge transfer co-crystals based on donor–acceptor interactions for near-infrared photothermal conversion, *Chem. Commun.*, 2020, **56**, 5223–5226.
22 K. P. Goetz, J. Tsutsumi, S. Pookpanratana, J. Chen, N. S. Corbin, R. K. Behera, V. Coropceanu, C. A. Richter, C. A. Hacker, T. Hasegawa and O. D. Jurchescu, Polymorphism in the 1:1 Charge-Transfer Complex DBTTF–TCNQ and Its Effects on Optical and Electronic Properties, *Advanced Electronic Materials*, 2016, **2**, 1600203.
23 J. Henderson, M. Masino, L. E. Hatcher, G. Kociok-Köhn, T. Salzillo, A. Brillante, P. R. Raithby, A. Girlando and E. Da Como, New Polymorphs of Perylene:Tetracyanoquinodimethane Charge Transfer Cocrystals, *Crystal Growth & Design*, 2018, **18**, 2003–2009.
24 B. W. D'Andrade, S. Datta, S. R. Forrest, P. Djurovich, E. Polikarpov and M. E. Thompson, Relationship between the ionization and oxidation potentials of molecular organic semiconductors, *Organic Electronics*, 2005, **6**, 11–20.
25 J. Cz. Dobrowolski, P. F. J. Lipiński and G. Karpińska, Substituent Effect in the First Excited Singlet State of Monosubstituted Benzenes, *J. Phys. Chem. A*, 2018, **122**, 4609–4621.
26 R. Oshi, S. Abdalla and M. Springborg, The impact of functionalization of organic semiconductors by electron donating groups on the reorganization energy, *Eur. Phys. J. D*, 2019, **73**, 124.
27 J. Tsutsumi, H. Matsui, T. Yamada, R. Kumai and T. Hasegawa, Generation and Diffusion of Photocarriers in Molecular Donor–Acceptor Systems: Dependence on Charge-Transfer Gap Energy, *J. Phys. Chem. C*, 2012, **116**, 23957–23964.
28 Y. Wu, Y. Zhen, Z. Wang and H. Fu, Donor-Linked Di(perylene bisimide)s: Arrays Exhibiting Fast Electron Transfer for Photosynthesis Mimics, *J. Phys. Chem. A*, 2013, **117**, 1712–1720.
29 K. Hu, Y. Gao, Y. Wang, Y. Yu, X. Zhao, S. A. Rotenberg, E. Gökmeşe, M. V. Mirkin, G. Friedman and Y. Gogotsi, Platinized carbon nanoelectrodes as potentiometric and amperometric SECM probes, *J Solid State Electrochem*, 2013, **17**, 2971–2977.
30 VesnaI. Basura, PaulD. Beattie and S. Holdcroft, Solid-state electrochemical oxygen reduction at Pt|Nafion® 117 and Pt|BAM3G^{TM} 407 interfaces, *Journal of Electroanalytical Chemistry*, 1998, **458**, 1–5.
31 R. Sainz, M. del Pozo, M. Vilas-Varela, J. Castro-Esteban, M. Pérez Corral, L. Vázquez, E. Blanco, D. Peña, J. A. Martín-Gago, G. J. Ellis, M. D. Petit-Domínguez, C. Quintana and E. Casero, Chemically synthesized chevron-like graphene nanoribbons for electrochemical sensors development: determination of epinephrine, *Sci Rep*, 2020, **10**, 14614.
32 M. Amelia, C. Lincheneau, S. Silvi and A. Credi, Electrochemical properties of CdSe and CdTe quantum dots, *Chem. Soc. Rev.*, 2012, **41**, 5728–5743.
33 J. Dhar, N. Venkatramaiah, A. A and S. Patil, Photophysical, electrochemical and solid state properties of diketopyrrolopyrrole based molecular materials: importance of the donor group, *J. Mater. Chem. C*, 2014, **2**, 3457–3466.
34 R. J. Walwyn, B. Chan, P. M. Usov, M. B. Solomon, S. G. Duyker, J. Y. Koo, M. Kawano, P. Turner, C. J. Kepert and D. M. D'Alessandro, Spectroscopic, electronic and computational properties of a mixed tetrachalcogenafulvalene and its charge transfer complex, *J. Mater. Chem. C*, 2018, **6**, 1092–1104.

35 Y. Wang, C. Zheng, W. Hao, H. Zhao, S. Li, L. Shen, J. Zhu and C.-A. Di, Impact of Stoichiometry and Fluorine Atoms on the Charge Transport of Perylene–F4TCNQ, *J. Phys. Chem. Lett.*, 2019, **10**, 3376–3380.
36 J. W. R. Macdonald, G. Piana, M. Comin, E. von Hauff, G. Kociok-Köhn, C. Bowen, P. Lagoudakis, G. D'Avino and E. D. Como, Charge transfer excitons in a donor–acceptor amphidynamic crystal: the role of dipole orientational order, *Mater. Horiz.*, 2020, **7**, 2951–2958.
37 S. Stoll and A. Schweiger, EasySpin, a comprehensive software package for spectral simulation and analysis in EPR, *Journal of Magnetic Resonance*, 2006, **178**, 42–55.
38 G. Kresse and J. Furthmüller, Efficient iterative schemes for \textit{ab initio} total-energy calculations using a plane-wave basis set, *Phys. Rev. B*, 1996, **54**, 11169–11186.
39 G. Kresse and D. Joubert, From ultrasoft pseudopotentials to the projector augmented-wave method, *Phys. Rev. B*, 1999, **59**, 1758–1775.
40 P. E. Blöchl, Projector augmented-wave method, *Phys. Rev. B*, 1994, **50**, 17953–17979.
41 A. Granovsky A., *Firefly version 8.0.0, http://classic.chem.msu.su/gran/firefly/index.html*, 2016.
42 M. W. Schmidt, K. K. Baldridge, J. A. Boatz, S. T. Elbert, M. S. Gordon, J. H. Jensen, S. Koseki, N. Matsunaga, K. A. Nguyen, S. Su, T. L. Windus, M. Dupuis and J. A. Montgomery, General atomic and molecular electronic structure system, *Journal of Computational Chemistry*, 1993, **14**, 1347–1363.
43 F. Neese, The ORCA program system, *WIREs Computational Molecular Science*, 2012, **2**, 73–78.
44 A. Kokalj, XCrySDen—a new program for displaying crystalline structures and electron densities, *Journal of Molecular Graphics and Modelling*, 1999, **17**, 176–179.
45 A. Kokalj, Computer graphics and graphical user interfaces as tools in simulations of matter at the atomic scale, *Computational Materials Science*, 2003, **28**, 155–168.
46 K. Momma and F. Izumi, VESTA 3 for three-dimensional visualization of crystal, volumetric and morphology data, *J Appl Cryst*, 2011, **44**, 1272–1276.
47 H. Q. Pham, Welcome to mcu's documentation! — mcu 0.2.beta documentation, https://hungqpham.com/mcu/index.html, (accessed June 27, 2022).
48 E. Sanville, S. D. Kenny, R. Smith and G. Henkelman, Improved grid-based algorithm for Bader charge allocation, *Journal of Computational Chemistry*, 2007, **28**, 899–908.
49 W. Tang, E. Sanville and G. Henkelman, A grid-based Bader analysis algorithm without lattice bias, *J. Phys.: Condens. Matter*, 2009, **21**, 084204.
50 G. Henkelman, https://theory.cm.utexas.edu/henkelman/research/bader/, (accessed May 31, 2022).
51 T. C. Werner, J. Chang and D. M. Hercules, Electrochemiluminescence of perylene. The role of direct excimer formation, *J. Am. Chem. Soc.*, 1970, **92**, 5560–5565.
52 F. Solano, P. Inaudi, M. Chiesa, G. Kociok-Köhn, E. Salvadori, E. Da Como, D. Vanossi, M. Malandrino, R. Carmieli, A. Giacomino and C. Fontanesi, Spin Multiplicity and Solid-State Electrochemical Behavior in Charge-Transfer Co-crystals of DBTTF/F4TCNQ, *J. Phys. Chem. C*, 2021, **125**, 8677–8683.
53 R. F. W. Bader, *Atoms in Molecules: A Quantum Theory*, Oxford University Press, Oxford, New York, 1994.